Sign of the nonlinear dielectric susceptibility of amorphous and crystalline $SrTiO_3$ films

S. Blonkowski,[1,*] E. Defay,[2] and X. Biquard[3]
[1]*STMicroelectronics, 850 Rue Jean Monnet, F-38926 Crolles, France*
[2]*CEA-LETI Minatec, 17 Rue des Martyrs, F-38054 Grenoble Cedex 9, France*
[3]*CEA-DSM/INAC/SP2M, 17 Rue des Martyrs, F-38054 Grenoble Cedex 9, France*
(Received 25 November 2008; published 19 March 2009)

Capacitance variation with electrical field and temperature of $SrTiO_3$ films based on metal-insulator-metal structures is shown to be opposite before and after crystallization. This motivates us to investigate the relationship between the crystallinity and the nonlinear dielectric susceptibility sign. Structural data (Extended X-Ray-Absorption Fine Structure and X-Ray Diffraction) are presented together with capacitance measurements as a function of static electric field and temperature. A statistical model shows that the nonlinear dielectric susceptibility sign results from the balance between short-range repulsive and long-range attractive interactions. The short-range interaction contribution to the nonlinear susceptibility depends on the anharmonic third-order term in the interionic potential energy, whereas the long-range contribution depends on the transverse effective charge logarithmic derivative against interionic distance. This last is found to be an increasing function of the transverse effective charge itself. The sign reversal between crystalline and amorphous $SrTiO_3$ is explained by the predominance of short-range contribution in the amorphous case and by the major long-range contribution reflected by the high transverse effective charge in the crystalline case. The consequences of the model are discussed in the cases of NaCl, CsCl, and the Curie temperature and constant of $BaTiO_3$.

DOI: 10.1103/PhysRevB.79.104108 PACS number(s): 77.22.−d, 77.84.Bw, 84.32.Tt

I. INTRODUCTION

The capacitance variations in perovskite metallic oxides based on metal-insulator-metal (MIM) capacitors [such as $SrTiO_3$ (STO), $PbZrTiO_3$, etc.] in the paraelectric phase present a concave shape with voltage alongside a decrease when temperature increases. The nonlinear susceptibility variation can be deduced from the Slater[1] model, extended by Barrett[2] for $SrTiO_3$. Analytical approximate expressions of the dielectric susceptibility variation with the field can be found in Refs. 3–5. In this case it is the positive fourth-order anharmonic term in the interionic potential energy which determines the variation in the dielectric nonlinear susceptibility.

However it has been reported that for low thermal budget deposited $SrTiO_3$ (below 450 °C),[6] the capacitance voltage variation is the opposite (i.e., convex) of the aforementioned case. Other low-temperature-deposited ABO_3 compounds based on MIM structures share this same capacitance voltage characteristic.[7] The same property is also generally observed for binary metallic oxides deposited at low-temperature MIMs.[8] This suggests that the nonlinear susceptibility sign of metallic oxides is correlated with their crystallinity. This motivates us to study the effect of the crystallinity on the nonlinear dielectric susceptibility of strontium titanate films as an example.

An experimental evidence of this correlation will be given by measurements of the capacitance variation in $Pt/SrTiO_3/Pt$ structures with voltage and temperature together with X-Ray Diffraction (XRD) and Extended X-Ray-Absorption Fine-Structure (EXAFS) measurements. Thereafter we will discuss the sign of the temperature and field variation in the dielectric susceptibility with the help of the Slater-Barrett models, where those variations are driven by a quartic anharmonic term in the interionic potential energy. Afterward the addition of the third-order anharmonic term will be introduced in the model. Comparison with our experimental data shows that the model is still not complete because those anharmonic terms are both deduced from short-range repulsive interactions. Finally a long-range term will be developed by using the contribution of the transverse effective charge. Its value will be compared to the fitted value from experimental data and discussed.

II. EXPERIMENTAL

STO thin films 50 nm and 200 nm thick are deposited on Pt bottom electrode by ion-beam sputtering (IBS), as described accurately elsewhere.[9] The main points of this deposition step are low working pressure (10^{-4} mbar) and low contamination as the substrate does not undergo the sputtering plasma. STO is deposited at room temperature and is amorphous just after deposition. It has been established by Rutherford backscattering that STO films are stoichiometric. Pt bottom electrode layer is 100 nm thick and is sputtered at 300 °C with pure argon. 20-nm-thick Ta or Ti is sputtered at ambient temperature with pure Ar underneath Pt and is used as a glue layer. When Ti is used, it is oxidized after deposition in a furnace at 600 °C in oxygen during 15 min. Classically, Ti or TiO_2 is used as a glue layer. However, as some EXAFS experiments are conducted at the Ti edge, a TiO_2 glue layer is avoided in this case in order to obtain Ti signal only from the STO layer. Therefore, samples observed at Sr edge are made with a TiO_2 glue layer, whereas samples observed at Ti edge are made with a Ta glue layer. This entire stack is deposited on oxidized standard Si wafers 525 μm thick with a diameter of 100 mm. The SiO_2 layer thickness is 500 nm. Crystallization is obtained by annealing the stack at 450 °C under air during 30 min. 100-nm-thick top electrode is made of Pt, sputtered at ambient temperature, and pat-

terned by using a lift-off technique in order to obtain square 0.01 mm^2 capacitors and contact electrodes. Samples were then mounted in a cryogenic prober system from Desert Cryogenics, LLC with a Lakeshore model 331 temperature controller. Capacitance C versus voltage characteristics presented here were measured with a HP-4194A impedance analyzer. A constant bias was superimposed on a small signal voltage of 30–40 mV amplitude at 100 kHz frequency. We do not observe significant capacitance dispersions with measurement frequencies.

X-ray absorption spectroscopy (XAS) experiments were performed at beamline FAME (BM30B) at the European Synchrotron Radiation Facility (ESRF) in Grenoble, France. XAS spectra were recorded at both the Ti K edge (4966 eV) and the Sr K edge (16 105 eV) in fluorescence mode with a 30 element energy-resolved detector. Experiments were conducted at room temperature, and the 200×300 μm^2 x-ray spot was kept centered on the $SrTiO_3$ sample (size $> 10 \times 10$ mm^2) during scans by dynamically adjusting the curvature of the second crystal of the Si monochromator and tracking the beam height. Good harmonic rejection and maximal resolution are achieved thanks to two Rh-coated mirrors of adjustable tilt and curvature located on both side of the monochromator. Incidence angle of the x-ray beam on the sample surface was kept constant at around $35° \pm 10°$. Energy calibration was made using Ti and Sr foils. Base line of XAS spectra was extracted using the ATHENA program[10] and EXAFS analysis was conducted using the FEFF and FEFFIT package programs.[11]

III. EXPERIMENTAL RESULTS

We have studied the crystalline STO layers obtained after annealing at 450–500 °C of amorphous STO deposited at temperature ranging from RT to 150 °C as well as nonannealed RT-deposited amorphous STO layer. Before annealing, STO films are amorphous according to θ-2θ diffraction diagrams showed in Fig. 1, whereas annealed STO is well crystallized in the perovskite phase. [Si (400) $\lambda/2$ is a measurement artifact due to Si substrate that is (100) oriented.]

Figure 2 shows the measured ratio $\Delta C/C = [C(T) - C(4\ \mathrm{K})]/C(4\ \mathrm{K})$ with C as the capacitance at 0 V versus temperature for amorphous and crystallized 50-nm-thick samples. For temperature above 70 K the variations in the samples are opposite. The amorphous STO sample presents a linear and positive capacitance variation with temperature, while the crystallized sample presents a decrease in capacitance with temperature similar to that observed in bulk single-crystal $SrTiO_3$.[12]

The values of the dielectric susceptibility extracted from 0 V capacitance at 4 K are 23 and 115 for the amorphous and crystallized samples, respectively. This last low value, compared to the bulk single-crystal STO,[12] has already been reported.[13] This is often explained by a dead-layer model with different physical interpretations[14] or by interfacial strain.[5] However this does not change the sign of the capacitance variation which is the purpose of the current work. The low-temperature broad peak around 40 K for the crystallized sample, which was also observed on sputtered thin films,[13]

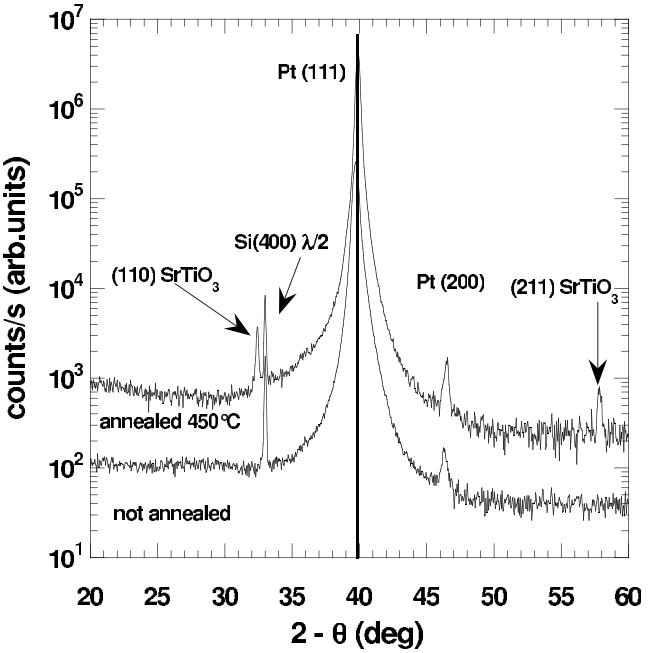

FIG. 1. θ-2θ XRD pattern of nonannealed and annealed (450 °C) $SrTiO_3$.

may be explained by the ac measuring field value. A 40 mV voltage on a thin sample (50 nm) induces an 8000 V/cm electrical field. With a field value of this level, a similar decrease in dielectric susceptibility was observed on bulk single-crystal STO (Ref. 12) at the same temperature range. If no significant field is applied, the flat shape of the single-crystal-reported dielectric susceptibility versus temperature below 40 K is well described by the Barrett theory.[2] In the case of the amorphous sample the dielectric susceptibility increases linearly with temperature.

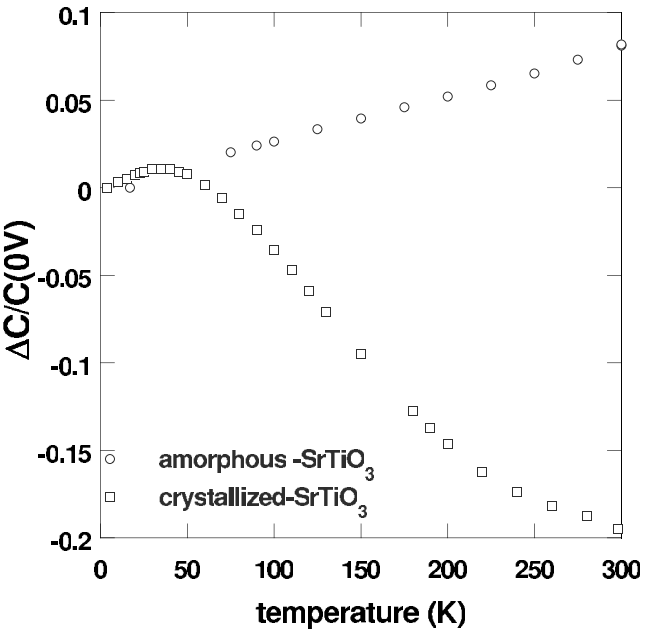

FIG. 2. Relative capacitance measured at 0 V defined as $[C(T) - C(4\ \mathrm{K})]/C(4\ \mathrm{K})$ vs temperature in K for amorphous (circles) and crystallized (squares) $SrTiO_3$.

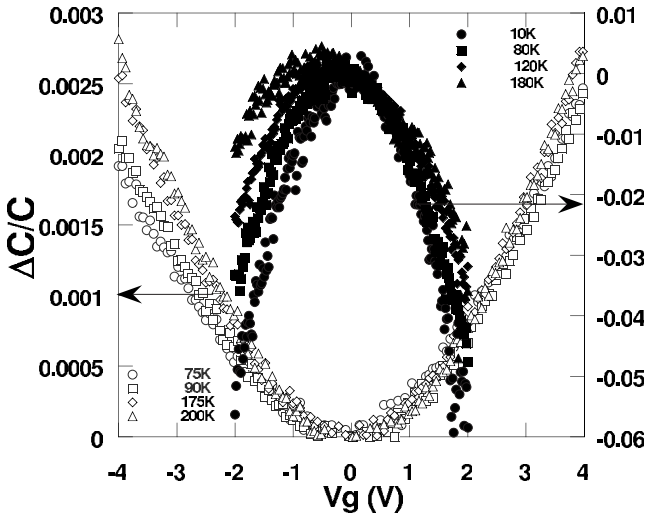

FIG. 3. Relative capacitance defined as $[C(V)-C(0)]/C(0)$ vs top electrode (gate) voltage in V for amorphous (open symbols) and crystallized (plain symbols) $SrTiO_3$ measured at different temperatures in K.

In Fig. 3 we reported the relative capacitance variations $\Delta C(V)/C(V)$ versus voltage V, defined as the ratio $[C(V) - C(0\ \mathrm{V})]/C(0\ \mathrm{V})$ where $C(V)$ and $C(0\ \mathrm{V})$ are the measured capacitances with applied voltage and at 0 V, respectively, at different temperatures. The convex variation in the amorphous sample capacitance is about ten times lower than the concave variation in the crystallized sample. The respective curvature sign of each sample is not changed with temperature.

In some cases, the convex variation can be explained by extrinsic phenomena, i.e., free charges where there is a polarization component resulting from space-charge effects. These charges can be electrons,[15] ions, or even vacancies.[16] Their quantity is thermally activated and this induces exponential capacitance variations with temperature. This is not observed in our case. Moreover the capacitance would exhibit a large variation with frequency which is also absent from our measurement. This indicates that the capacitance variations observed are not consistent with the space-charge effect but are more likely related to the nonlinear dielectric susceptibility itself. This hypothesis is supported by the comparison between XRD spectra and capacitance measurements which shows a correlation between the material structure long-range order and dielectric susceptibility variations. In the case of alkali halides the dielectric susceptibility variation with temperature was explained by Havinga and Bosman[17] in terms of the first-neighbor atoms. This point will be discussed in Secs. IV B and IV D. In the current study, the quantity and nature of the atom first neighbors were deduced from EXAFS measurements.

For crystalline $SrTiO_3$, recorded spectra at both Sr and Ti edge, were found to be undistinguishable from the $SrTiO_3$ powder spectra as shown in Fig. 1. XRD studies also showed that annealed $SrTiO_3$ layer is perovskite. Following Wyckoff,[18] Sr atoms have 12 O at 2.76 Å as first neighbors, whereas Ti atoms are located inside an octahedron made of 6 O at 1.95 Å.

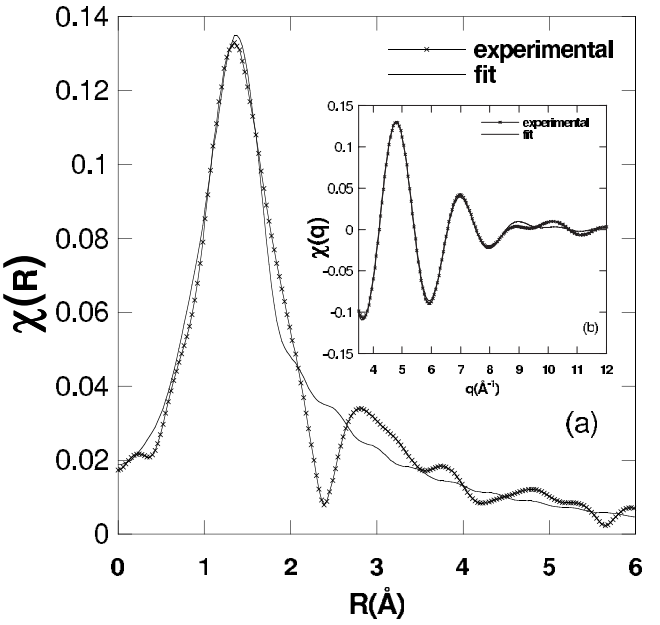

FIG. 4. EXAFS oscillations of amorphous $SrTiO_3$ at the Ti edge. Data are represented by a line with crosses while the fitting is the continuous line. χ(R) is not phase corrected.

Figures 4 and 5 show the Fourier transform $|\chi(R)|$ of the EXAFS oscillations $\chi(k)$ (not shown here) for Ti and Sr, respectively. The k value is in the range $[3.45-10.3\ \mathrm{Å}^{-1}]$ for Ti and in the range $[2.6-11.6\ \mathrm{Å}^{-1}]$ for Sr. $\chi(k)$ rapidly decreasing intensity indicates that Ti and Sr are immediately surrounded by a light element which is O. This dominant contribution gives rise to the main peak on the $|\chi(R)|$ diagram at the pseudodistance 1.9 Å for Sr and 1.3 Å for Ti. Only this dominant contribution was taken into account for

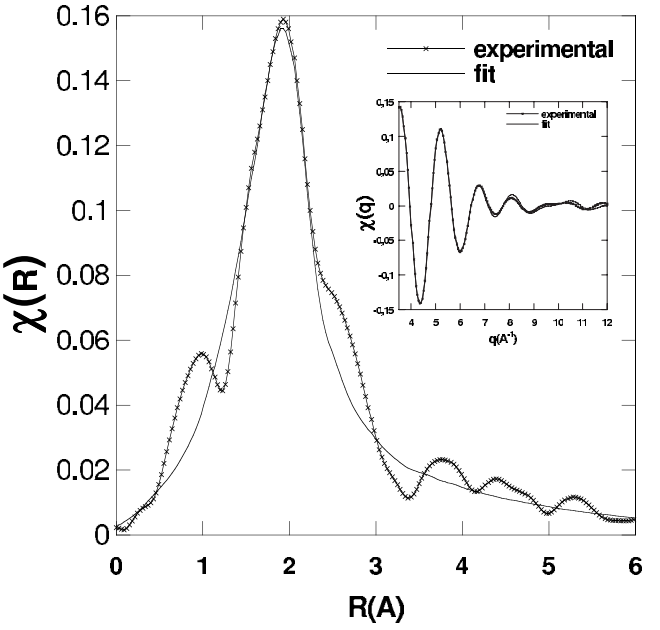

FIG. 5. EXAFS oscillations of amorphous $SrTiO_3$ at the Sr edge. Data are represented by a line with crosses while the fitting is the continuous line. χ(R) is not phase corrected.

TABLE I. Adjustment values for data fit of amorphous STO. S_0^2 was fixed to 0.8. For crystalline $SrTiO_3$, distances, nature, and number values were taken from crystallographic tables.

	R range for back transform	Nature	Number	Distance (Å)
Around Ti	[0.5:1.9]			
First-neighbor amorphous STO		Oxygen	3.4 ± 0.4	1.87 ± 0.01
Crystalline $SrTiO_3$			6	1.95
Around Sr	[1.2:2.4]			
First-neighbor amorphous STO		Oxygen	6.5 ± 0.4	2.52 ± 0.01
Crystalline $SrTiO_3$			12	2.76

the fitting, which was conducted on the Fourier back-transformed oscillations $\chi(q)$ as illustrated in the insets of Figs. 4 and 5. Fitting is given in Table I.

The number of O atoms around Ti is close to four, which is in line with a tetrahedral environment. For Sr, the number of O is close to six at 2.52 Å, thus similar to the SrO structure where Sr is surrounded by six O at 2.58 Å.

To summarize, XAS studies show that during the STO phase change from amorphous to crystalline, Sr and Ti stay surrounded by O and both experience an increase in the quantity of the surrounding O and an increase in the distance between them and O. Ti undergoes a tetrahedral-to-octahedral transition associated with a 4% distance lengthening, whereas Sr first neighbors jump from 6 to 12 with a large (10%) lengthening in distance.

IV. DISCUSSION

A. Statistical Slater-Barrett models

The question of the low-frequency dielectric susceptibility variation with field and temperature can be treated in the framework of statistical mechanics. In the case of perovskites, Slater-Barrett models[1,2] provide useful approximate expressions. In this section we will highlight how the statistical models can describe both the dielectric susceptibility variation with temperature and field. The basis of those models consists in computing the free energy of the positive ions in an energy potential ϕ expanded in power series with respect to the relative ionic displacement (in Cartesian coordinates x_α) and to the electric field E (in Cartesian coordinates E_α),

$$\phi = \phi_0 + a\sum_\alpha^3 x_\alpha^2 + b\sum_\alpha^3 x_\alpha^4 - \sum_\alpha^3 qE_\alpha x_\alpha. \tag{1}$$

Here, the problem is described in the frame of quantum mechanics. Then, from the previous potential, a Hamiltonian operator H is introduced,

$$H = \frac{P_\alpha^2}{2m} + a\sum_\alpha^3 X_\alpha^2 + b\sum_\alpha^3 X_\alpha^4 - \sum_\alpha^3 qE_\alpha X_\alpha. \tag{2}$$

X_α and P_α stand for position and impulsion operators, respectively. By definition, the partition function Z_H is the trace of the quantum operator $Z_H = \mathrm{Tr}(e^{-H/kT})$,[19] where k is the Boltzmann constant and T is the temperature. The first-order eigenvalues of H are calculated with the help of the perturbation theory.[20] For a system of N identical ions, the Helmholtz free energy A_E is given by

$$A_E = -kT \ln\left(\frac{Z_H^N}{N!}\right). \tag{3}$$

In this case the free energy takes the form

$$A_E = A_{E0} - \frac{K}{2}\sum_\alpha^3 E_\alpha^2 + \frac{S}{4}\sum_\alpha^3 E_\alpha^4, \tag{4}$$

with

$$K = \frac{Nq^2}{2a}\left[1 + 3\frac{\hbar\omega}{2a^2}\coth\left(\frac{\hbar\omega}{2kT}\right)[-b]\right], \tag{5a}$$

$$S = \frac{Nq^4}{4a^4}(b), \tag{5b}$$

$$A_{E0} = NkTLn\left[\frac{N}{e}2\sinh\left(\frac{\hbar\omega}{2kT}\right)^3\right] + \frac{9Nb}{16a^2}(\hbar\omega)^2\coth\left(\frac{\hbar\omega}{2kT}\right)^2. \tag{5c}$$

The entropy Σ_E given by $\Sigma_E = -\partial A_E/\partial T$ has the following expression at high temperature:

$$\Sigma_E = Nk\ln\left[\frac{e}{Nh^3}(\pi kT)^3\left(\frac{2m}{a}\right)^{3/2}\right] + 3Nk - \frac{9Nk^2T}{2a^2}(b) + \frac{3kNq^2}{4a^3}\sum_\alpha^3 E_\alpha^2(-b). \tag{6}$$

As explained by Slater,[1] Eq. (6) shows the entropy dependence on the restoring force constant, a. For a large value of a, the ion is confined to a small volume. If the volume available is reduced the entropy is reduced too. From the stationary perturbation theory[20] the b term increases the energy levels if b is positive. For a given energy, the number of available states must be lower and the entropy is reduced too.

Consequently, as $(\partial^2\Sigma_E/\partial E^2)_T = (\partial\chi/\varepsilon_0\partial T)_E$, according to Eq. (6), χ (the dielectric susceptibility) decreases with temperature since b is positive. Let us consider, as an illustration, the example of free rotating dipoles. Applying a field tends to align the dipoles, resulting in an entropy reduction.

This in turn decreases the dielectric susceptibility with temperature. The temperature dependence of the dielectric susceptibility is the same as the entropy dependence on the electric field. Since b is positive, it is not possible to explain the positive variations observed for the noncrystallized samples.

Taking into account the Lorentz correction due to Slater which is expressed by coefficients C_1-C_5 (Ref. 1) and assuming that the polarization and the applied field are parallel to direction α, the Slater Model leads to the following equations:

$$E_\alpha = P_\alpha\left[\frac{1}{K}\left(\frac{C_3}{C_5}\right)^2 + \frac{C_4C_3}{C_5^2\cdot\varepsilon_0}\right] + \frac{S}{K^4}\left(\frac{C_3}{C_5}\right)^4 P_\alpha^3, \quad (7a)$$

$$\frac{1}{\chi(E,T)\varepsilon_0} = \frac{1}{K}\left(\frac{C_3}{C_5}\right)^2 + \frac{C_4C_3}{C_5^2\cdot\varepsilon_0} + \frac{3.S}{K^4}\left(\frac{C_3}{C_5}\right)^4 P_\alpha^2, \quad (7b)$$

where ε_0 is the vacuum permittivity, as P_α and χ are the ionic part of the polarization and the dielectric susceptibility, respectively. It is worth noting that the C_i coefficients depend only on the electronic polarizabilities of Sr, Ti, and O. The low-frequency part of the dielectric permittivity, ε, is given by

$$\varepsilon - \varepsilon_\infty = \frac{\frac{K}{\varepsilon_0}\left(\frac{C_5}{C_3}\right)^2}{1+\frac{K}{\varepsilon_0}\left(\frac{C_4}{C_3}\right)}, \quad (8)$$

where ε_∞ is the optical dielectric constant. Note that for a homogeneous amorphous sample one can expect that the Lorentz field is correct ($C_3=3/(\varepsilon_\infty+2)$, $C_5=1$, and $C_4=-1/3$) and does not affect the sign of K and S.

Inserting this expression of K in Eq. (8) gives the Barrett expression[2] with only one b term. Only one term was used for the sake of simplicity. This simplification does not affect the relevance of the discussion. The K factor temperature dependence accounts well for the $\varepsilon(T)$ characteristics of $SrTiO_3$

The resolution of Eqs. (7) and (8) provides the temperature and field dependence of the dielectric susceptibility (and then the capacitance per surface unit $C=\varepsilon\varepsilon_0/d$ where d is the film thickness) through the expressions of K and S. One can observe that the temperature variations $\varepsilon(T)$ are driven by the sign of K whereas the curvature of $\varepsilon(E)$ is fixed by the sign of S. Both depend on the same microscopic anharmonic b term according to Eqs. (5a) and (5b). Hence temperature and field dielectric susceptibility variations have the same physical origin. This is observed in Figs. 2 and 3 where the signs of the capacitance variations versus temperature and field both change with the $SrTiO_3$ crystalline state. The values of the b anharmonic microscopic parameter alone is not sufficient to fit the experimental $C(V)$ and $C(T)$ characteristics of Figs. 2 and 3.

B. Third-order anharmonicity

Havinga and Bosman[17] dealt with a similar question in the case of alkali halide crystals. The dielectric constant-temperature dependence of alkali halides in the NaCl and CsCl structures were found to be opposite, i.e., positive for NaCl and negative for CsCl crystalline structures. They have developed a model also based on the classic statistical treatment of an interionic potential. But their approach contains a third-order term in the expansion of this potential. Using a more elaborate treatment based on normal coordinates, they have shown that this third-order term accounts for the positive variations in the dielectric susceptibility of alkali halides in the NaCl structure. This term which represents the fluctuations acts via the square of the third-order term multiplied by the number of the first neighbors. If one introduces such a third-order term in the expansion of Eq. (1), it becomes

$$\phi = \phi_0 + a\sum_\alpha^3 x_\alpha^2 + c\sum_\alpha^3 x_\alpha^3 + b\sum_\alpha^3 x_\alpha^4 - \sum_\alpha^3 qE_\alpha x_\alpha. \quad (9)$$

This gives the following Hamiltonian:

$$H = \frac{P_\alpha^2}{2m} + a\sum_\alpha^3 X_\alpha^2 + c\sum_\alpha^3 X_\alpha^3 + b\sum_\alpha^3 X_\alpha^4 - \sum_\alpha^3 qE_\alpha X_\alpha. \quad (10)$$

The following derivation is essentially similar to the one presented in Sec. IV A. From the quantum-mechanics perturbation expansion, the c term decreases the oscillators energy levels by terms proportional to c^2.[20] So that for a given energy the number of states is increased by the third-order term, leading to entropy increase. Finally the introduction of the c term modifies the terms K and S of Sec. IV A which become

$$K = \frac{Nq^2}{2a}\left\{1 + 3\frac{\hbar\omega}{2a^2}\coth\left(\frac{\hbar\omega}{2kT}\right)\left[\frac{3c^2}{2a}f(T) - b\right]\right\}, \quad (11a)$$

$$S = \frac{Nq^4}{4a^4}\left(b - \frac{9c^2}{4a}\right), \quad (11b)$$

where $f(T)$ is a continuous increasing function of temperature,

$$f(T) = \frac{1}{4}\left\{3 + \frac{\hbar\omega}{2kT}\left[\coth\left(\frac{\hbar\omega}{2kT}\right) - th\left(\frac{\hbar\omega}{2kT}\right)\right]\right\}. \quad (11c)$$

Note that $f(T)\sim 1$ in the high-temperature domain (i.e., typically above 100 K). Besides the c coefficient of this model is directly linked to the value of the linear thermal-expansion coefficient γ_L. Using the same statistical model, one can obtain $\langle x\rangle \approx -(3ck/4a^2)T$ at the high-temperature limit and then the linear coefficient of expansion is $\gamma_L=-3ck/4a^2R$, with R being the first-neighbor distance. The c coefficient can now be readily replaced in Eqs. (11a) and (11b) by a function of γ_L which is a measurable quantity. From Eqs. (11a)–(11c), it is clear that the c^2 term counteracts the b term, leading to an entropy increase. Since c is proportional to γ_L this entropy increase represents the dipole-moment length fluctuations.

Since a, b, and c result from the serial expansion of the potential energy, Φ, K, and S can be evaluated. Indeed, if Φ is assumed to be the sum of a repulsive radial Born A/R^l

potential and an attractive $-B/R^p$ potential one has $\Phi(R)=(A/R^l)-(B/R^p)$. In this case, taking into account the equilibrium condition $\partial\Phi/\partial R=0$, the anharmonic terms are given by

$$a=\frac{\partial^2\Phi}{2\,\partial R^2}=A\frac{l(l-p)}{R^{l+2}},\quad c=\frac{\partial^3\Phi}{3\,!\,\partial R^3}=-\frac{a(l+2)}{3R},$$

$$b=\frac{\partial^4\Phi}{4\,!\,\partial R^4}=\frac{a(l+2)(l+3)}{12R^2}. \tag{12}$$

From Eq. (11a) (for temperatures typically above 100 K) the sign of K, and then of the temperature dependence of the dielectric susceptibility, is the sign of $[(3c^2/2a)-b]$. From Eq. (12) one has $[3c^2/2a\approx 2b]$ and the dielectric susceptibility must increase with temperature. In the Havinga and Bosman[17] treatment the fluctuation term is weighted by a function of the first-neighbor number z and the sign of K is the sign of $[(3c^2/2a)(3.15/z-1)-b]$. Using again Eq. (12), the sign of K is negative if $z>7$. It follows that for CsCl, because $z=8$, the dielectric susceptibility decreases with temperature, whereas the opposite variation was observed for NaCl for which $z=6$. From those considerations and taking into account that there are six first neighbors for Ti in the crystallized samples as measured by EXAFS and 3.4 first neighbors for Ti in the amorphous sample (see Table I) both crystalline and amorphous $SrTiO_3$ dielectric susceptibility should increase with temperature. Another physical effect should play a role.

C. Nonlinear transverse effective charge

Let us consider now the temperature variation in the transverse optic mode frequency, ω_{TO}. Its square is the difference between a short-range-order term ω_0 and a long-range-order term ω_{DD} characterizing the dipole-dipole interactions, that is to say

$$\omega_{TO}^2=\omega_0^2-\omega_{DD}^2. \tag{13}$$

Since ω_0^2 represents the short-range mechanical frequency it must vary with interatomic distance as R^{-l}, with l typically above 8 for a Born potential. The long-range term is given by[21,22]

$$\omega_{DD}^2=\frac{Ne_T^{*2}}{\mu\varepsilon_0(\varepsilon_\infty+2)}, \tag{14}$$

Where e_T^* is the transverse effective charge, μ is the reduced mass of the oscillator, and N is the oscillator density. Assuming that the interatomic distance increases linearly with temperature, ω_{TO}^2 should decrease with temperature, thanks to the R dependence of ω_O^2 in Eq. (13). However, it has been established experimentally that ω_{TO}^2 increases with temperature for crystalline $SrTiO_3$.[23] As the dielectric susceptibility is inversely proportional to ω_{TO}^2 (via the Lyddane-Sachs-Teller relationship), the same conclusion than the previous thermodynamic model can be drawn. Here again, the short-range interactions cannot account for the observed temperature dependence of the dielectric susceptibility. Nevertheless this example is instructive. The transverse effective charge

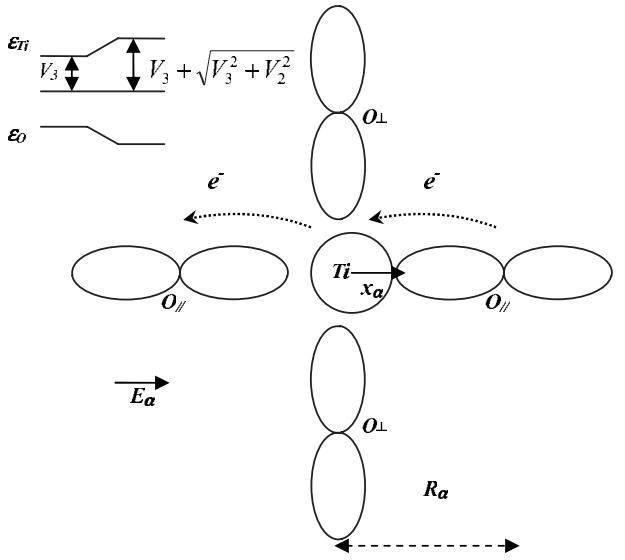

FIG. 6. Illustration of the BOM model for the electronic dipole arising from central cation displacement.

can be defined as the spatial derivative of the dipolar moment of a crystal cell.[24] It is then reasonable to consider that the transverse effective charge depends also on the interatomic distance. Differentiation of Eq. (13) following this assumption gives $\partial\omega_{TO}^2/\partial T\propto[\omega_0^2(\partial Ln(\omega_0)/\partial Ln(R))-\omega_{DD}^2(\partial Ln(e_T^*)/\partial Ln(R))]$. The first logarithmic derivative is negative, then the $\partial Ln(e_T^*)/\partial Ln(R)$ term must be negative in order to account for $\partial\omega_{TO}^2/\partial T\geq 0$, as observed experimentally.[23]

As shown by Harrison[25,26] within the framework of the bond orbital model (BOM), the charge has two contributions. On one hand, the effective charge Z^* is static and results from the coupling energy between atomic individual states. On the other hand, a dynamic contribution is due to the dipole moment induced by the displacement x_α of an atom. The sum of both contributions is called the transverse effective charge e_T^*. First, we want to expand to the second order, according to the atomic displacement, the Ti effective transverse charge using a simplified BOM approach. As shown in Fig. 6 we consider a two-state BOM model. Let V_3 be the difference between the energy of the individual states ε_{Ti} and ε_O and V_2—the coupling between these states. If the Ti ion has z O first neighbors, the static contribution from the BOM model is $Z^*\cong Z-2z(V_2^2/4V_3^2)$ which is lower than the nominal ionic charge Z. Here all the charges are in electronic charge unit and the factor 2 accounts for the two electronic spin values. According to the BOM model and Fig. 6, the Ti displacement x_α changes the coupling with the atom $O_\parallel$ on the left, resulting in a charge-transferred $\delta Q=-x_\alpha(d/dR)(V_2^2/4V_3^2)-(x_\alpha^2/2)(d^2/dR^2)(V_2^2/4V_3^2)$. Assuming that V_2 varies as $1/R^n$, one obtains a dipole moment $P=R\delta Q$ where $P=(x_\alpha/2)(nV_2^2/V_3^2)-x_\alpha^2(n(2n+1)/R)(V_2^2/4V_3^2)$. There is the same transfer from Ti to the $O_\parallel$ atom on the right. Taking into account the two spins, the dynamic contribution is $4P/x_\alpha$ and the total effective charge is

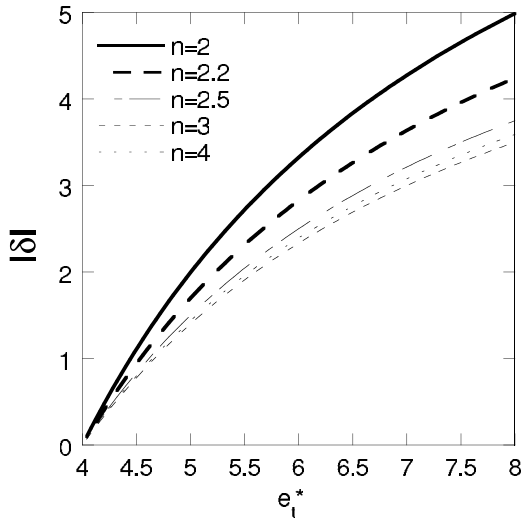

FIG. 7. Absolute value of δ as a function of e_T^* following Eq. (17) for several values of the exponent n.

$$e_T^*(x_\alpha) = Z + \left\{ \frac{V_2^2}{V_3^2}\left(2n - \frac{z}{2}\right) - \frac{n(2n+1)x_\alpha}{R}\frac{V_2^2}{V_3^2} \right\}, \quad (15)$$

Note that

$$e_T^* = Z + \left\{ \frac{V_2^2}{V_3^2}\left(2n - \frac{z}{2}\right) \right\}. \quad (16)$$

Expressing V_2^2/V_3^2 as a function of e_T^*, Eq. (15) can therefore be written as

$$e_T^*(x_\alpha) = e_T^* - \frac{2n(2n+1)x_\alpha}{R}\left(\frac{e_T^* - Z}{4n - z}\right), \quad (17a)$$

in the same way

$$Z^* = Z - \frac{z}{2}\left(\frac{e_T^* - Z}{4n - Z}\right). \quad (17b)$$

The parameter δ, the transverse effective charge logarithmic derivative, is given by

$$\delta = \frac{R}{e_T^*}\frac{de_T^*}{dR} = \frac{\partial Ln(e_T^*)}{\partial Ln(R)} = -\frac{2n(2n+1)}{(4n-z)}\left(\frac{e_T^* - Z}{e_T^*}\right). \quad (18)$$

Since e_T^* is larger than Z, δ is negative for $n > z/4$, and $|\delta|$ is an increasing function of e_T^* according to Eq. (18). This is illustrated in Fig. 7 for several values of the exponent n ($2 < n < 4$) and will be discussed in Sec. IV D.

D. Statistical model with the nonlinear effective transverse charge

The effective transverse charge is defined for a null macroscopic field. The charge relevant in the statistical model, q, is defined for a null local field and both are related by $q = e_T^*/\Lambda$ where Λ is the local-field correction factor[24] [$\Lambda = (\varepsilon_\infty + 2)/3$ when the Lorentz field is applicable]. Note that δ does not depend on Λ. The Lorentz field correction (due to the effect of the $O_\parallel$ electronic polarization) derived by Slater is, according to his original notation, C_5/C_3 and then $q = e_T^* C_3/C_5$. (Here we keep the same values for $C_3 = 0.385$, $C_5 = 1.241$, and $C_4 = -2.076$ which is equivalent to approximate Sr electronic polarizability to the one of Ba.)

From Eqs. (17) and (18) we obtain

$$q(x_\alpha) = q + \frac{x_\alpha \delta q}{R}. \quad (19)$$

The presence of an electric field results in the addition of the term $-[\Sigma_\alpha q E_\alpha x_\alpha + \delta(q/R)E_\alpha x_\alpha^2]$ in Eq. (9). However the charge is not the ionic charge, Z^*, displaced as a whole with the ion. In this last case the equilibrium position in presence of a field is $x = Z^* E/2a$. If we consider the transverse effective charge $x = e_T^* E/2a$ so that the equilibrium position is enhanced by a factor e_T^*/Z^*. One has then to rescale a, by the factor e_T^*/Z^*. This holds also for b and c. In the following we will note that $a_T = a(e_T^*/Z^*)$, $b_T = b(e_T^*/Z^*)$, and $c_T = c(e_T^*/Z^*)$. Taking this into account Eq. (9) becomes

$$\phi = \phi_0 + a_T \sum_\alpha^3 x_\alpha^2 + c_T \sum_\alpha^3 x_\alpha^3 + b_T \sum_\alpha^3 x_\alpha^4 - \sum_\alpha^3 \left(q E_\alpha x_\alpha + \frac{\delta q}{R} E_\alpha x_\alpha^2 \right). \quad (20)$$

The process in Sec. IV A can also be applied by using Eq. (20) instead of Eq. (9). The only change is the quadratic term that becomes $a_T - \Sigma_\alpha(\delta q/R)E_\alpha$. The rest of the calculation is similar to Sec. IV B with the Hamiltonian

$$H = \frac{P_\alpha^2}{2m} + a_T \sum_\alpha^3 X_\alpha^2 + c_T \sum_\alpha^3 X_\alpha^3 + b_T \sum_\alpha^3 X_\alpha^4 - \sum_\alpha^3 \left(q E_\alpha X_\alpha + \frac{\delta q}{R} E_\alpha X_\alpha^2 \right). \quad (21)$$

After a derivation similar to the one of Sec. IV B using the perturbation theory, the δ term in the Hamiltonian increases the oscillator energy levels by terms proportional to $c_T\delta$. Indeed, since δ and c_T are negative the product $c_T\delta$ should be positive. As discussed in the beginning of Sec. IV A, at a given energy those terms reduce the number of available states and then the entropy. The expressions of K and S become

$$K = \frac{Nq^2}{2a_T}\left\{ 1 + 3\frac{\hbar\omega}{2a_T^2}\coth\left(\frac{\hbar\omega}{2kT}\right)\left[\left(\frac{3c_T^2}{2a_T} - 2c_T\frac{\delta}{R} \right) f(T) - b_T \right] \right\}, \quad (22a)$$

$$S = \frac{Nq^4}{4a_T^4}\left(b_T + 6c_T\frac{\delta}{R} - \frac{9c_T^2}{4a_T} \right). \quad (22b)$$

In Eqs. (22a) and (22b), the term $c_T\delta$ represents the coupling between the dipole-moment size fluctuation and the charge transfer. If the dipole is dilated, the transferred charge is reduced, and conversely if the dipole is compressed the charge transfer is enhanced. This coupling between the charge transfer and the dipole size reduces the dipoles moment fluctuations and then the entropy.

TABLE II. Calculated and fitted parameters for crystalline STO. The first column contains several values of the repulsive short-range potential power-law exponent. The second gives the values of $a=-(l+2)k/4\gamma_L R^2$ in eV/Å^2. the third column gives the value of Z^* with the help of the fitted value of a_T from the $\varepsilon(T)$ characteristic and the value of $e_T^*=7.26$ (Ref. 24). The last three columns give the values of n and Z^* from Eq. (17b) and δ from Eq. (18).

l	a (eV/Å^2)	$Z^*=e_T^* a/a_T$	n [Eq. (17b)]	Z^* [Eq. (17b)]	δ [Eq. (18)]
6	4.8	0.845	3.05	0.85	−3.12
8	6.0	1.05	3.15	1.045	−3.12
10	7.2	1.26	3.29	1.28	−3.13
12	8.4	1.47	3.40	1.43	−3.13

From Eq. (22a) and taking into account that $b_T \sim 3c_T^2/4a_T$, the sign of K is the same as the sign of $[-(3c_T R/4a_T)+\delta]=[-(3cR/4a)+\delta]$ in the high-temperature domain. Defining the Grüneisen constant as[26] $\gamma_G=-(R/6a)(da/dR)$, the sign of K is the sign of $[(3\gamma_G/4)+\delta]$.

From Eq. (18) of Sec. IV C we have $\delta=-[2n(2n+1)/(4n-z)](e_T^*-Z/e_T^*)$. For NaCl with $n=2$ we have then $\delta_{\mathrm{NaCl}}=-10[(e_T^*-Z)/e_T^*]$. For a CsCl structure a similar calculation as in Sec. IV C gives $\delta=-[n(2n+1)/(2n-3)](2/\sqrt{3})[(e_T^*-Z)/e_T^*]$. For $n=2$ we have then $\delta_{\mathrm{CsCl}}=-(20/\sqrt{3})[(e_T^*-Z)/e_T^*]$. Now $e_T^*=1.11$ for NaCl and $e_T^*=1.31$ for CsCl.[21] Whence $\delta_{\mathrm{NaCl}}=-0.99$ and $\delta_{\mathrm{CsCl}}=-2.73$. Moreover $\gamma_{\mathrm{NaCl}}=1.5$ and $\gamma_{\mathrm{CsCl}}=2.1$,[27] then the term $[(3\gamma_G/4)+\delta]$ is equal to 0.13 for NaCl and −1.15 for CsCl. From this it results that K and then the temperature variation in the dielectric susceptibility are positive for NaCl and negative for CsCl. This is in agreement with the experimental results.[17]

Returning now to $SrTiO_3$ using Eqs. (7) and (8) and the expressions of K and S from Eqs. (22a) and (22b), it is now possible to fit the $C(V)$ and $C(T)$ characteristics from Figs. 2 and 3. In this calculation, $N=(2R)^{-3}$ for one Ti ion in a cubic cell. The R and z values are taken from EXAFS data reported in Table I (note that there are no differences between crystallized thin films and bulk crystal values). Concerning the crystalline sample it is more accurate to fit the single-crystal values from Ref. 12 in order to avoid errors arising from the thin-film dead-layer effect (this does not modify however the sign of the dielectric permittivity variation). In this case $e_T^*=7.26$,[24] so $q=e_T^* C_3/C_5=2.25$ is fixed. It is worth noticing that the charge $q=2.25$ is lower than the nominal charge $Z=+4$ for Ti. (In the original Slater and Barrett models the charge is assumed to be the ionic charge that follows the ion in its motion so that the ionic polarizability results from the displaced charge as a whole. However this charge was already evaluated closer to $Z=+1$ than the expected nominal charge for Ti, $Z=+4$, because the harmonic term a behaves like 7.6 eV/Å$^2\times Z^2$.[1] This discrepancy is solved in our model.)

The harmonic term a is fixed (as a function of the potential-energy exponent l), consistent with our statistical approach to the thermal-expansion coefficient with $\gamma_L=-3ck/4a^2R$. One can define $\gamma_{LT}=-3c_T k/4a_T^2 R$. Taking into account Eq. (12), $a=-[(l+2)k]/4\gamma_L R^2$ or $a_T=-[(l+2)k]/4\gamma_{LT}R^2$. If one uses the experimental value of $\gamma L=9.4\times10^{-6}$ K^{-1},[28] the only parameters to extract from the $\varepsilon(T)$ characteristic fit are a_T and δ [because of Eq. (12)]. The fitted values are $a_T=41.24$ eV/Å^2 and $\delta=-3.15$. These values have to be compared with the results of Eqs. (17b) and (18) which give the value of Z^* and δ as a function of n. Because a depends on l we have reported the results on Table II for several values of l $(6<l<12)$ in the second column. The values $4.8<a<8.4$ in eV/Å^2 present a correct order of magnitude. In the third column we have reported the values of Z^* deduced from the fits [taking $e_T^*=7.26$ (Ref. 24)]. In the last three columns of Table II the results of Eqs. (17b) and (18) are reported. The values of n must range between 3 and 3.4 in order to give Z^* values consistent with the fits. These values are in good agreement with the value of $n=7/2$ used in Ref. 24 in order to calculate e_T^* for $SrTiO_3$. The calculated values of δ (last column of Table II) are not very sensitive to the exponent n in the range given in Table II. This is illustrated in Fig. 7 where $\delta(e_T^*)$ is plotted [Eq. (18)] for several values of n. δ is very weakly sensitive to n when $2.5<n<4$ and in good agreement with the fitted value (−3.1), whatever the value of l. However $|\delta|$ increases strongly with e_T^*. Note that $|\delta|\sim0$ when $e_T^*\sim Z$. The effect of δ on the $\varepsilon^{-1}(T)$ characteristics is illustrated in Fig. 8. When $|\delta|$ decreases the $\varepsilon^{-1}(T)$ slope decreases until it changes its sign (for $\delta\sim-1.5$). Then one expects a lower value of $|\delta|$ in the case of amorphous $SrTiO_3$.

In this last case the fitted $C(V)$ and $C(T)$ characteristics are those corresponding to Figs. 2 and 3. The fits take into account the R and z from EXAFS as reported in Table I. However neither γ_L nor e_T^* is known. The parameters a_T, δ, and e_T^* will be fitted. We will assume that the Lorentz field will apply for homogenous amorphous material and then $q=3e_T^*/(\varepsilon_\infty+2)$. The results of the fits are compared to the results of Eq. (17) and (18). Moreover there is a slight difference between the $C(V)$ and $C(T)$ fits which may be attributed to thin-film effects (i.e., dead layer). However this does not alter the sign and the order of magnitude of the fitted parameters which are presented in Table III. The agreement between the fitted values and calculated values of δ and e_T^* is good for $n=4$. The ratio e_T^*/Z^* is ~1 then $a_T\sim a$. In this case the classic ionic model is valid. The δ parameter is lower by 1 order of magnitude than in the case of crystalline $SrTiO_3$. The short-range restoring force dominates, resulting in an increase in the dielectric susceptibility with field and temperature. The difference between amorphous and crystalline $SrTiO_3$ is according to Eqs. (16) and (18) (illustrated in

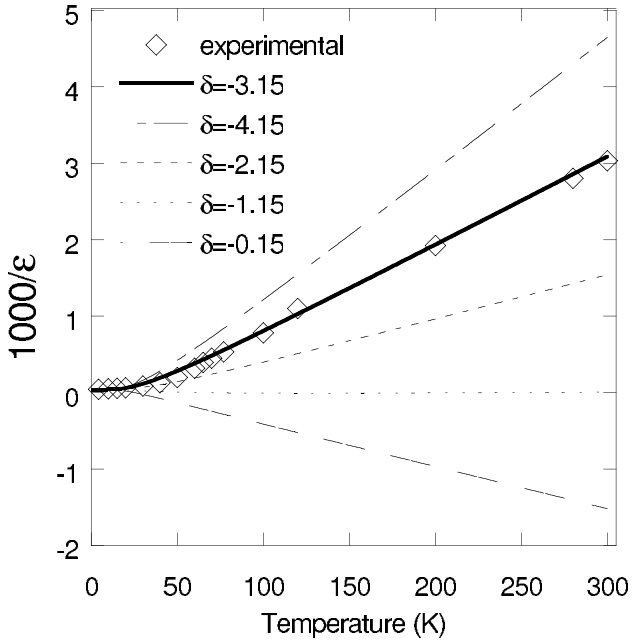

FIG. 8. Inverse of the dielectric susceptibility vs temperature in K for bulk crystalline $SrTiO_3$ in the {1,0,0} direction Ref. 12. Experimental (squares) and calculated (line) curves are plotted with a_T=41.24 eV/Å^2 several values of δ.

Fig. 7) due to the magnitude of the transverse effective charge. The latter is much larger (7.26) in the crystalline state than in the amorphous state (4.1–4.2). The magnitude of the transverse effective charge in both phases could however be computed with the help of *ab initio* calculations.

As a final remark one can obtain from Eqs. (8) and (22a) at high temperature a Curie-Weiss law,

$$\varepsilon - \varepsilon_\infty = \frac{M}{T - T_0}, \tag{23}$$

where

$$M = \frac{C_5^2}{8C_3C_4\gamma_{LT}\left(\frac{3\gamma_G}{4} + \delta\right)} \tag{24}$$

and

$$T_0 = -\frac{\left[1 + \frac{2a_T\varepsilon_0C_3}{Nq^2C_4}\right]}{8\gamma_{LT}\left(\frac{3\gamma_G}{4} + \delta\right)} = -\frac{MC_3C_4}{C_5^2}\left[1 + \frac{2a_T\varepsilon_0C_3}{Nq^2C_4}\right]. \tag{25}$$

Note that Eq. (24) shows that the Curie constant M is inversely proportional to the thermal-expansion coefficient as in the Cochran theory of ferroelectricity.[29] (This is mainly due to the introduction of the third-order term in the Slater-Barrett approaches). From Eqs. (24) and (25) one can readily express a necessary condition for the ferroelectric transition occurrence $[(3\gamma_G/4)+\delta]<0$. The magnitude of δ has to be large enough in order to make T_0 and M positive. According to Eqs. (16) and (18) the magnitude of δ increases with the coupling energy V_2 which represents the hybridization between Ti and its O neighbors. The necessary condition for ferroelectric transition, consistent with the interpretation of Cohen and Krakauer,[30] translates the importance of the Ti-O hybridization.

For $BaTiO_3$, the experimental values are $M \sim 1.7.10^5$ K, $T_0 \sim 120$ °C,[31,32] and $\gamma_L \sim 9.8\times10^{-6}$ K^{-1}.[33] The numerical resolution of Eqs. (24) and (25) taking into account Eqs. (17b) and (18) allows one to calculate e_T^* with l and n as parameters. We find from the resolution of Eqs. (24) and (25) for l=8 and n=2.9 that e_T^*=6.7 and e_T^*=7.3, respectively [corresponding, respectively, to δ=−2.9 and δ=−3.2 from Eq. (18)]. This is the good order of magnitude since $6.7 < e_T^* < 7.51$ in the cubic phase.[24]

V. CONCLUSION

Comparing XRD and capacitance measurements, we have shown that the $SrTiO_3$ dielectric susceptibility variations with electric field and temperature change their sign according to their amorphous or crystalline state. Those variations were first analyzed with a statistical model of an ion in an anharmonic potential accounting for short-range interactions. The third-order anharmonic term in this potential is predominant. It lowers the individual harmonic-oscillator energy levels, enhancing the number of available states. This effect enhances the entropy and then the dielectric susceptibility when the temperature or the electric field is increased. This is consistent with the observed positive variations in the dielectric susceptibility as observed for amorphous $SrTiO_3$. However, this model is unable to explain the negative variations in the dielectric susceptibility for the crystalline $SrTiO_3$. To improve the model, a nonlinear long-range interaction term

TABLE III. Calculated and fitted parameters for amorphous STO. The first three columns correspond to the fitted values [on $C(V)$ in the first line and $C(T)$ in the second line] of a_T and e_T^* via $q=3e_T^*/(\varepsilon_\infty+2)$ and δ. The last three columns contain for comparison the results of e_T^* calculated with Eq. (17a), δ calculated with Eq. (18), and Z^* [Eq. (17b)] for the same value of n=4.

	a_T (eV/Å^2)	e_T^*	δ	e_T^* [Eq. (18)] (n=4)	δ [Eq. (17a)] (n=4)	Z^* [Eq. (17b)] (n=4)
$C(V)$	4.5	4.2	−0.4	4.2	−0.6	3.93
$C(T)$	5.2	4.1	−0.6			

is added to the previous potential. It is expressed by the logarithmic derivative of the transverse effective charge against the interionic distance, δ. This long-range-order term increases the harmonic-oscillator energy levels, reducing the number of available states. This effect reduces the entropy and then the dielectric susceptibility when the temperature or the electric field increases.

From a dipole-moment point of view, the effect of δ is to change the charge in the dipole moment whereas the short-range harmonic term reflects the dipole-length variation. When the dipoles are expanded, their charge is reduced and when the dipoles are compressed their charge is enhanced. When increasing, this charge transfer decreases the dipole-moment fluctuations and then the entropy, leading in turn to decrease the dielectric susceptibility with temperature and applied field.

We derived independently an analytic approximate expression of δ, which is an increasing function of the transverse effective charge itself. Using the statistical model, this calculated value of δ was shown to be in good agreement with the experimental dielectric susceptibility variations in crystalline $SrTiO_3$. In this case, the large value of δ results from the large transverse effective charge of the perovskite structure. Conversely the value of δ in the amorphous state is found to be much lower, suggesting that the effective transverse charge is lower. In this case the dielectric susceptibility variations are mainly due to short-range interactions. The model proposed here shows that the dielectric susceptibility variations sign with temperature may be approximate by the sign of $[(3\gamma_G/4)+\delta]$, with γ_G being the Grüneisen constant. As a result this sign is found to be positive for NaCl and negative for CsCl, which corresponds to the experimental dielectric susceptibility variations with temperature. Moreover, an approximate expression of the Curie constant and temperature is consistent with the experimental values for $BaTiO_3$.

ACKNOWLEDGMENTS

The authors are thankful to J. Guillan for her help in the early stage of this work, to F. Ferrieu for providing ellipsometric measurements, to V. Nassif, O. Proux, H. Palacher, D. Jalabert, and G. Rolland for their help in managing the beamline, to C. Lhaule and F. Hippert for giving beamline time during the Ti-edge experiment, to F. Mondon for very fruitful discussions, and to C. Gagne and A. Pemberton for their help in the English version improvement of this paper.

*serge.blonkowski@cea.fr

[1] J. C. Slater, Phys. Rev. **78**, 748 (1950).
[2] J. H. Barrett, Phys. Rev. **86**, 118 (1952).
[3] O. G. Vendik and S. P. Zubko, Tech. Phys. **42**, 278 (1997).
[4] J. M. Worlock and P. A. Fleury, Phys. Rev. Lett. **19**, 1176 (1967).
[5] A. Antons, J. B. Neaton, K. M. Rabe, and D. Vanderbilt, Phys. Rev. B **71**, 024102 (2005).
[6] K. C. Chiang, Ching-Chien Huang, G. L. Chen, Wen Jauh Chen, H. L. Kao, Yung-Hsien Wu, Albert Chin, and Sean P. McAlister, IEEE Trans. Electron Devices **53**, 2312 (2006).
[7] L. Goux, H. Vander Meeren, and D. J. Wouters, J. Electrochem. Soc. **153**, F132 (2006).
[8] S. Blonkowski, Appl. Phys. Lett. **91**, 172903 (2007).
[9] J. Guillan, G. Tartavel, E. Defaÿ, L. Ulmer, L. Galéra, B. André, and F. Baume, Integr. Ferroelectr. **67**, 93 (2004).
[10] B. Ravel and M. Newville, J. Synchrotron Radiat. **12**, 537 (2005).
[11] J. J. Rehr and R. C. Albers, Rev. Mod. Phys. **72**, 621 (2000).
[12] R. C. Neville, B. Hoeneisen, and C. A. Mead, J. Appl. Phys. **43**, 2124 (1972).
[13] H. M. Christen, J. Mannhart, E. J. Williams, and Ch. Gerber, Phys. Rev. B **49**, 12095 (1994).
[14] S. P. Keane, S. Schmidt, J. Lu, A. E. Romanov, and S. Stemmer, J. Appl. Phys. **99**, 033521 (2006).
[15] S. Blonkowski, M. Regache, and A. Halimaoui, J. Appl. Phys. **90**, 1501 (2001).
[16] P. Gonon and C. Vallée, Appl. Phys. Lett. **90**, 142906 (2007).
[17] E. E. Havinga and A. J. Bosman, Phys. Rev. **140**, A292 (1965).
[18] R. W. G. Wyckoff, *Crystal Structures* Second Edition, (Krieger Publishing Company, Florida, 1986), Vol. II, p. 390.
[19] L. Landau and E. Lifchitz, *Physique Théorique: Physique Statistique* (MIR, Moscou, 1967), Vol. 5.
[20] C. Cohen-Tanoudji, B. Diu, and F. Laloe, *Mecanique quantique, tome 2*, Hermann, (1973) Paris.
[21] G. Lucovsky, R. M. Martin, and E. Burstein, Phys. Rev. B **4**, 1367 (1971).
[22] G. V. G. Baonza, M. Taravillo, M. Caceres, and J. Nunez, Phys. Rev. B **73**, 214117 (2006).
[23] J. M. Worlock and P. A. Fleury, Phys. Rev. Lett. **19**, 1176 (1967).
[24] P. Ghosez, J.-P. Michenaud, and X. Gonze, Phys. Rev. B **58**, 6224 (1998).
[25] W. A. Harrison, Phys. Rev. B **74**, 205101 (2006).
[26] W. A. Harrison, *Elementary Electronic Structure: Revised Edition* (World Scientific, Singapore, 2004).
[27] J. E. Rapp and H. D. Merchant, J. Appl. Phys. **44**, 3919 (1973).
[28] F. W. Lytle, J. Appl. Phys. **35**, 2212 (1964).
[29] W. Cochran, Adv. Phys. **9**, 387 (1960).
[30] R. E. Cohen and H. Krakauer, Phys. Rev. B **42**, 6416 (1990).
[31] F. Jona and G. Shirane, *Ferroelectric Crystals* (Pergamon, Oxford, 1962).
[32] G. Shirane and A. Takeda, J. Phys. Soc. Jpn. **7**, 1 (1952).
[33] M. Liu, T. R. Finlayson, and T. F. Smith, Phys. Rev. B **55**, 3480 (1997).